Thu. Nov 12, 2020

Room E

[1E01-03] International sess. 1

Chair:Toru Murayama(Tokyo Metropolitan University)
9:30 AM - 10:30 AM Room E (3F/Conf. Room E1-2)

[1E01] Nano-catalyst engineering for storage and release of hydrogen energy using formic acid as a promising liquid carrier
○Kohsuke Mori[1] (1. Graduate School of Engineering, Osaka University)
9:30 AM - 10:00 AM

[1E02] **CO_2-to-Methanol Hydrogenation Catalyst by Focusing on Coordination Structure of Cu species**
○Shohei Tada[1], Fumito Otsuka[2], Ryuji Kikuch[2] (1. Ibaraki University, 2. The University of Tokyo)
10:00 AM - 10:15 AM

[1E03] Effects of supports for Pt-based catalysts on conversion of lignocellulosic biomass into aromatic monomers in supercritical water
○Kiyoyuki Yamazaki[1], Ryuto Sasaki[2], Tatsuya Watanabe[2], Satoko Kuwano[2], Naoki Mimura[1], Osamu Sato[1], Aritomo Yamaguchi[1] (1. National Institute of Advanced Industrial Science and Technology, 2. Tohoku Gakuin University)
10:15 AM - 10:30 AM

[1E04-06] International sess. 2

Chair:Takuya Yoshikawa(Tokyo Metropolitan University)
10:45 AM - 11:30 AM Room E (3F/Conf. Room E1-2)

[1E04] Role of acid sites for selective catalytic oxidation of NH_3: the case of niobium oxide supported precious metals catalysts
○Mingyue Lin[1], Baoxiang An[1], Takashi Takei[1], Tetsuya Shishido[1], Tamao Ishida[1], Masatake Haruta[1], Toru Murayama[1,2] (1. Tokyo Metropolitan University, 2. Yantai University)
10:45 AM - 11:00 AM

[1E05] **Reductive Amination of HMF over Beta Zeolite-supported Ruthenium bimetallic Catalyst**
○Xinyue Li[1], Son Dinh Le[1], Shun Nishimura[1] (1. Japan Advanced Institute of Science and Technology)
11:00 AM - 11:15 AM

[1E06] Reaction mechanism of dechlorination of chlorofluoroalkene by hydrogen gas over intermetallic compound catalysts
○Tomoaki TAKAYAMA[1], Satoshi ARIYAMA[1], Taku YAMADA[2], Takayuki KOMATSU[1] (1. Tokyo Institute of Technology, 2. AGC Inc.)
11:15 AM - 11:30 AM

[1E07-09] International sess. 3

Chair:Tomoaki TAKAYAMA(Tokyo Institute of Technology)
1:00 PM - 2:00 PM Room E (3F/Conf. Room E1-2)

[1E07] Development of Ni-Ir alloy catalyst for hydrogenation of unsaturated compounds
○Masazumi Tamura[1] (1. Osaka City University)
1:00 PM - 1:30 PM

[1E08] Hydroxyapatite supported polyvinylpyrrolidone-capped CuPd bimetallic catalyst for highly selective γ-butyrolactone *via* hydrogenation of succinic acid
○Son Dinh Le[1], Shun Nishimura[1] (1. Graduate School of Advanced Science and Technology, Japan Advanced Institute of Science and Technology)
1:30 PM - 1:45 PM

[1E09] Ultrastable and selective catalyst for propane dehydrogenation using Pb-modified PtGa alloy
Yuki Nakaya[1], Ken-ichi Shimizu[1], ○Shinya Furukawa[1] (1. Institute for Catalysis, Hokkaido University)
1:45 PM - 2:00 PM

[1E10-11] International sess. 4

Chair:Shun Nishimura(Japan Advanced Institute of Science and Technology)
2:15 PM - 3:00 PM Room E (3F/Conf. Room E1-2)

[1E10] Synthesis of zeolitic Mo-doped vanadotungstate materials with tailorable oxidability and acidity
○Meilin Tao[1], Satoshi Ishikawa[1], Wataru Ueda[1] (1. Faculty of engineering, department of material and life chemistry, Kanagawa University)
2:15 PM - 2:30 PM

[1E11] Development of nano-structured catalyst using oxide nanosheets
○Shintaro Ida[1] (1. Institute of Industrial Nanomaterials, Kumamoto University)
2:30 PM - 3:00 PM

International sess.

[1E01-03] International sess. 1

Chair:Toru Murayama(Tokyo Metropolitan University)

Thu. Nov 12, 2020 9:30 AM - 10:30 AM Room E (3F/Conf. Room E1-2)

[1E01] Nano-catalyst engineering for storage and release of hydrogen energy using formic acid as a promising liquid carrier

○Kohsuke Mori[1]（1. Graduate School of Engineering, Osaka University）

9:30 AM - 10:00 AM

[1E02] **CO_2-to-Methanol Hydrogenation Catalyst by Focusing on Coordination Structure of Cu species**

○Shohei Tada[1], Fumito Otsuka[2], Ryuji Kikuch[2]（1. Ibaraki University, 2. The University of Tokyo）

10:00 AM - 10:15 AM

[1E03] Effects of supports for Pt-based catalysts on conversion of lignocellulosic biomass into aromatic monomers in supercritical water

○Kiyoyuki Yamazaki[1], Ryuto Sasaki[2], Tatsuya Watanabe[2], Satoko Kuwano[2], Naoki Mimura[1], Osamu Sato[1], Aritomo Yamaguchi[1]（1. National Institute of Advanced Industrial Science and Technology, 2. Tohoku Gakuin University）

10:15 AM - 10:30 AM

Nano-catalyst Engineering for Storage and Release of Hydrogen Energy Using Formic Acid as a Promising Liquid Carrier

(Osaka Univ.[*]・ESICB Kyoto University[**]) ○Kohsuke Mori[*,**]

1. Introduction

Formic acid (FA, HCOOH) has emerged as one of the most promising hydrogen storage compounds because it has a high gravimetric capacity for hydrogen (4.4 wt%), is relatively nontoxic and is a nonflammable liquid under ambient conditions. Additionally, the use of FA could allow economical CO_2-mediated hydrogen storage energy cycling via the regeneration of FA through the hydrogenation of CO_2. Thus the development of reliable heterogeneous catalysts targeted to both FA dehydrogenation and FA synthesis is an urgent yet challenging task. Herein the state of the art in the exploitation of promising nano-catalysts designed by surface and interface engineering with atomic precision for this targeted reaction are presented, which further provides the precise catalytic site design protocols.

2. Hydrogen production from FA

The decomposition of FA by selective dehydrogenation ($HCOOH \rightarrow H_2 + CO_2$) is thermodynamically favored ($\Delta G = -48.4$ kJ mol^{-1}). It is desirable to completely suppress the side reaction $HCOOH \rightarrow CO + H_2O$ ($\Delta G = -28.5$ kJ mol^{-1}), because the generated CO is both highly toxic and capable of poisoning Pt fuel cell catalysts. For the practical reason of on-board application, current research has been focused on the exploitation of efficient heterogeneous catalysts. Bering this in mind, we have developed the heterogeneous nano-catalysts, such as PdAg, PdAu, PdCu, PdCuCr, for the efficient production of high-purity H_2 from FA dehydrogenation [1-5].

PdAg nanoparticles supported on phenylamine-functionalized mesoporous carbon (MSC) were synthesized as a heterogeneous catalyst (**Fig. 1A**) [6]. The PdAg NPs were evidently well dispersed and had a narrow size distribution, with an average diameter of 1.2 nm (**Fig. 1B**). The Pd 3d peaks in XPS analysis generated by the PdAg/amine-MSC was shifted to lower binding energies than that of the corresponding monometallic Pd catalysts. This outcome is attributed to the ability of Ag atoms to donate electrons to Pd atoms after alloying, based on their electronegativity values of 1.93 and 2.20.

A remarkably high turnover frequency (TOF) of 5638 h^{-1} was obtained during the dehydrogenation of FA, corresponding to an outstanding reaction rate of 1,070,000 mL·h^{-1}·g$_{Pd}$$^{-1}$. It should be noted that the present catalytic system can suppress unfavorable CO contamination from the dehydration pathway ($HCOOH \rightarrow H_2O + CO$) less than detection limit by GC (1 ppm). The Ag catalyst did not show any activity (data not shown), while the catalytic performance of the PdAg was higher than that of the monometallic Pd analogue (**Fig. 1C**).
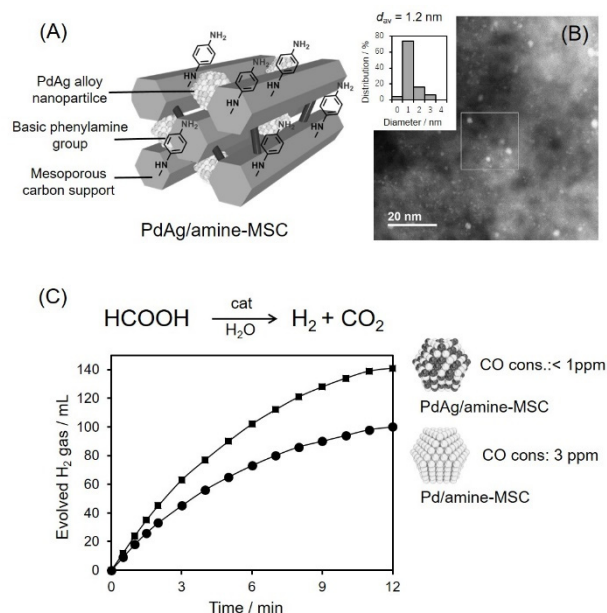

Fig. 1 (A) Illustartion of PdAg/amine-MSC, (B) HAADF-STEM image and size distribution plot, and (C) time profile in the FA dehydrogenation.

In the dehydrogenation of FA, the reaction is initiated by the O-H bond cleavage to form metal-formate species (Step 1) (**Fig. 2**). Such metal-formate species undergo the isomerization (Step 2), and evolve metal hydride and CO_2 via β-hydride elimination (Step 3). The catalytic cycle concludes with the regeneration of the catalysts accompanied with the formation of H_2 (Step 4). To better understand the role of the amine functional groups and the alloying, potential energy profiles were generated using DFT calculations, employing a $Pd_{11}Ag_{11}$ cluster as a model for alloy NPs.

In the presence of phenylamine, the formation of HCOOH–$PhNH_2$ appears reasonable as a result of the acid-base interaction, and $HCOO^-$ is spontaneously generated without any transition state. On the other hand,

the activation energy was deteremiend to 11.9 kcal/mol to produce the formate (HCOO⁻) intermediate in the absence of amine group. Moreover, H_2 production occurs with a barrier of 7.8 kcal/mol in the presence of phenylamine, which is substantially lower than the value of 23.0 kcal/mol calculated in the absence of the amine. It can be concluded that both the O–H bond dissociation and the H_2 desorption steps are enhanced by the presence of neighboring amine functional groups.

The activation energies for each elementary steps over the Pd22 cluster model were determined to be 20.0, 15.2, 16.6 and 24.6 kcal/mol for steps 1 – 4, respectively. Alloying Pd with Ag changes the electron density at the active Pd sites due to charge transfer from Ag to Pd resulting from the different work functions of the two elements, which facilitate the O–H and C–H bond dissociation steps. Kinetic Isotope Effect (KIE) using HCOOH, HCOOD and DCOOH also support such results.
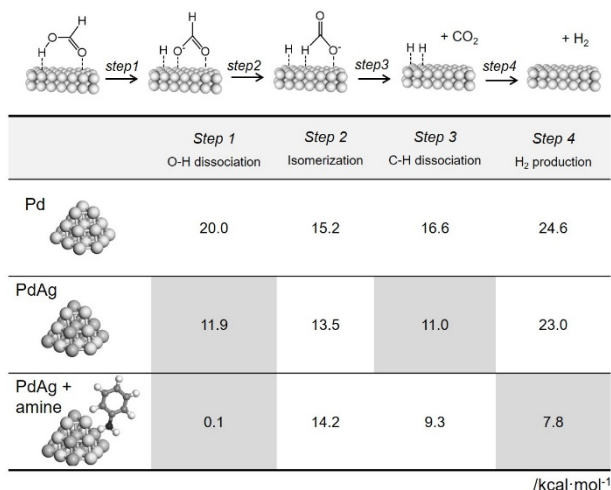

	Step 1 O-H dissociation	Step 2 Isomerization	Step 3 C-H dissociation	Step 4 H₂ production
Pd	20.0	15.2	16.6	24.6
PdAg	11.9	13.5	11.0	23.0
PdAg + amine	0.1	14.2	9.3	7.8

/kcal·mol⁻¹

Fig. 2 A possible reaction pathway and activation enetgies for dehydrogenation to FA over Pd22 and Pd11Ag11 cluster models determined by DFT calculations.

More recently, we demonstrate the selective production of hydrogen isotope compounds from a combination of formic acid and D_2O, through cooperative action by a PdAg nanocatalyst on a silica substrate whose surface is modified with amine groups (**Fig. 3**) [7]. In this process, D_2 is predominantly evolved by the assist of weakly basic amine moieties, while nanocatalyst particles in the vicinity of strongly basic amine groups promote the preferential formation of HD. Kinetic data and calculations based on semi-classically corrected transition state theory coupled with density functional theory suggest that quantum tunneling dominates the hydrogen/deuterium exchange reaction over the metallic PdAg surfaces.
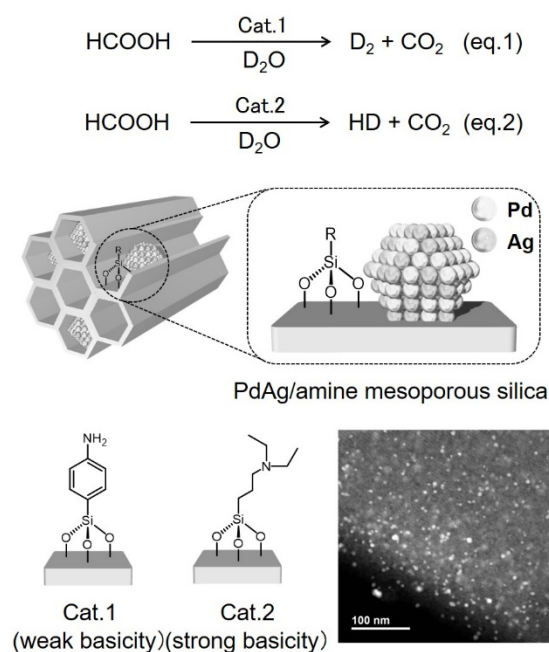

Fig. 3 Controlled release of hydrogen isotope compounds from the dehydrogenation of FA in D_2O using amine functionalized PdAf catalyst.

3. FA synthesis from CO₂ Hydrogenation

The gas phase hydrogenation of CO_2 to produce formic has a positive free energy change (CO_2 (g) + H_2 (g) → HCOOH (l), ΔG = +33 kJ mol⁻¹). Conventionally, the reaction is performed in an aqueous condition by the addition of a weak base, such as a tertiary amine or alkali/alkaline earth bicarbonate, which enable the shift of thermodynamic equilibrium to the product side (CO_2 (aq) + H_2 (aq) + B → HCO_2^- (aq) + BH^+ (B: base), ΔG = −35.4 kJ mol⁻¹) [8]. Unfortunately, the advance of heterogeneous catalysts lags considerably in spite of the noticeable practical benefits even in the industrial application.

The precise tuning of the surface composition of PdAg nanoparticles was performed to investigate the effect of surface-exposed active Pd atoms in alloy NPs [9]. The co-reduction of Pd and Ag precursors conventionally afford random PdAg alloy nanoparticles (PdAg/TiO_2) By applying a surface engineering approach via the successive reduction of metal precursors, Pd@Ag/TiO_2 with a $Pd_{core}Ag_{shell}$ structure and Ag@Pd/TiO_2 with an $Ag_{core}Pd_{shell}$ structure were synthesized.

PdAg alloy nanoparticles supported on TiO_2 was proven to be an efficient selective hydrogenation catalyst of CO_2 100 °C under relatively low pressure condition (2.0 MPa, CO_2/H_2 =1). The Pd@Ag/TiO_2 exhibited an

elevated TON (2,496) based on the total quantities of Pd employed despite the low density of surface exposed Pd atoms. As expected, a maximum TON value of 14839 was obtained from the Pd@Ag/TiO$_2$ based on the quantity of surface Pd atoms, which was determined by pulsed CO adsorption measurements, This TON value is a more than ten times higher than that of the monometallic Pd/TiO$_2$. Moreover, a well correlation between the TON based on surface Pd atoms and the Pd 3d$_{5/2}$ binding energy determined by XPS analysis evidently observed.
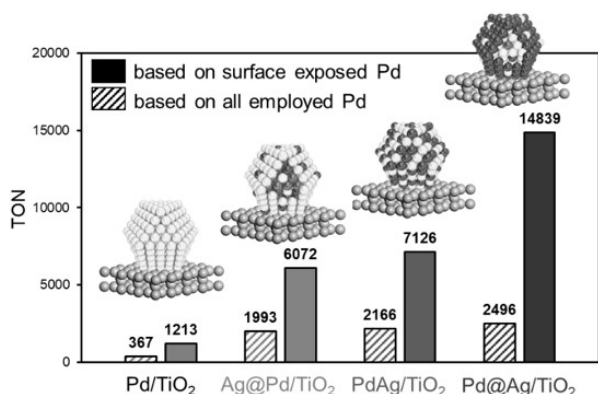

Fig. 4 Comparison of the catalytic activities of a series of supported PdAg catalysts with different surface compositions and Pd/TiO$_2$ during CO$_2$ hydrogenation.

The CO$_2$ hydrogenation over Pd$_{22}$ is initiated by the dissociation of H$_2$ to form a metal-hydride species via TS$_{I/II}$ with a barrier of 13.9 kcal/mol (*step 1*). Next, the adsorption of HCO$_3^-$ to produce intermediate III (*step 2*), followed by the attack of H atom to the C atom of HCO$_3^-$ via TS$_{III/IV}$, with a barrier of 77.4 kcal/mol (*step 3*). Finally, the formate is produced accompanied by H$_2$O regenerates the initial active species (*step 4*). The activation energies for *step 1* using Pd$_{11}$Ag$_{11}$ and Pd$_6$Ag$_{16}$ clusters, were 11.9 and 11.0 kcal/mol, respectively, which were similar to that obtained with the Pd$_{22}$. On the other hand, the reduction of HCO$_3^-$ via TS$_{III/IV}$ occurs with a barrier of 58.7 and 46.2 kcal/mol for Pd$_{11}$Ag$_{11}$ and Pd$_6$Ag$_{16}$, respectively. These results show that the rate-determining step is *step 3*, and further demonstrate that the importance of low Pd/Ag ratio of the PdAg alloy nanoparticles in boosting the rate-determining step.

We have recently elucidated the positive effects imparted by the interfacial modification of PdAg/TiO$_2$ with ZIF-8 during CO$_2$ hydrogenation to FA [10, 11]. Moreover, a PdAg catalyst on a hydrophilic N-doped polymer-silica composite support was proven to be active for the CO$_2$ hydrogenation reaction under additive-free aqueous conditions to produce pure formic acid (CO$_2$ (aq) + H$_2$ (aq) → HCOOH (aq), ΔG = −4 kJ mol^{-1}) [12]. High hydrophilic nature and the higher CO$_2$ adsorption capacity at low temperatures compared to metal oxide supports may have contributed to the increased activity.
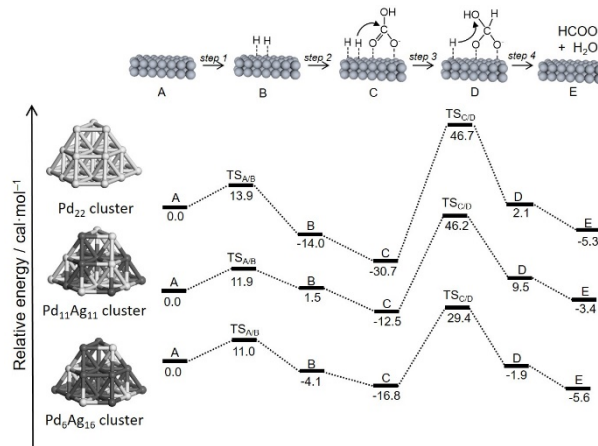

Fig. 5 Possible reaction mechanism for CO$_2$ hydrogenation to formic acid and potential energy profiles as determined by DFT calculations.

1) K. Mori, M. Dojo, H. Yamashita, *ACS Catal.*, **3**, 1114 (2013).
2) K. Mori, H. Tanaka, M. Dojo, K. Yoshizawa, H. Yamashita, *Chem. Eur. J.*, **21**, 12085 (2015).
3) K. Mori, K. Naka, S. Masuda, K. Miyawaki, H. Yamashita, *ChemCatChem*, **9**, 3456 (2017).
4) K. Mori, S. Masuda, H. Tanaka, K. Yoshizawa, M. Che, H. Yamashita, *Chem. Commun.*, **53**, 4677 (2017).
5) M. Wen, K. Mori, Y. Kuwahara, H. Yamashita, *ACS Energy Lett.*, 2, 1 (2017).
6) S. Masuda, K. Mori, Y. Futamura, H. Yamashita, *ACS Catal.*, **8**, 2277 (2018).
7) K. Mori, Y. Futamura, S. Masuda, H. Kobayashi, H. Yamashita, *Nat. Commun.*, **10**, 4094 (2019).
8) K. Mori, T. Taga, H. Yamashita, *ACS Catal.*, **7**, 3147 (2017).
9) K. Mori, T. Sano, H. Kobayashi, H. Yamashita, *J. Am. Chem. Soc.*, **140**, 8902 (2018).
10) M. Wen, K. Mori, Y. Futamura, Y. Kuwahara, M. Navlani-García, T. An, and H. Yamashita, *Sci. Rep.*, **9**, 15675 (2019).
11) K. Mori, A. Konishi, H. Yamashita, *J. Phys. Chem. C*, **124**, 11499 (2020).
12) S. Masuda, K. Mori, Y. Kuwahara, C. Louis, H. Yamashita, *ACS Appl. Energy Mater.*, **3**, 5847 (2020).

CO$_2$-to-methanol hydrogenation catalyst by focusing on coordination structure of Cu species

(Ibaraki Univ. *, Univ. Tokyo**) ○Shohei Tada*, Fumito Otsuka**, Ryuji Kikuchi**

1. Introduction

Recently, the catalyst development for CO$_2$ hydrogenation to methanol has attracted attention. Many researchers have been investigating Cu-based catalysts to improve catalytic activity. We focused on the metal nanoparticle formation by the deposition-reduction method. After H$_2$ reduces the metal-containing mixed oxides, the metal nanoparticles will be selectively formed. We considered that a spinel-type oxide Mg$_{1-x}$Cu$_x$Al$_2$O$_4$ is a promising catalyst specific to the CO$_2$ hydrogenation. It is a basic metal oxide, which can activate CO$_2$ adsorbed on its surface. Furthermore, it has a high specific surface area, which will increase the number of active sites.

In this study, we investigated the mechanism of Cu nanoparticle formation *via* the deposition-reduction method over Mg$_{1-x}$Cu$_x$Al$_2$O$_4$.

2. Experimental

Mg$_{1-x}$Cu$_x$Al$_2$O$_4$ was prepared by the Pechini method. Ethylene glycol (Wako) and citric acid (Sigma-Aldrich) were stirred at 200 °C and homogenized. The molar ratio of ethylene glycol to citric acid was 4. Stoichiometric amounts of Mg(NO$_3$)$_2$·6H$_2$O (Wako), Al(NO$_3$)$_3$·9H$_2$O (Wako), Cu(NO$_3$)$_2$·3H$_2$O (Wako) were added to the obtained solution at 80 °C. The solution was heated at 200 °C, resulting in the powder formation. The crude powder was calcined at 800 °C for 4 h. The obtained catalysts were characterized by temperature-programmed reduction of H$_2$ (H$_2$-TPR), ^{27}Al MAS-NMR, XAS, and EPR.

3. Results and Discussion

H$_2$-TPR was conducted using Mg$_{1-x}$Cu$_x$Al$_2$O$_4$ to evaluate their reducibility (Figure 1). First, we estimated their Cu loading assuming that the peak corresponds to Cu^{2+} reduction to Cu^0. The Cu loading is almost the same as that calculated from the stoichiometric ratio of Cu to Mg and Al, namely x, as summarized in Table 1. Therefore, we can conclude that the peak corresponds to the reduction of Cu^{2+}. Second, we focused on the low-temperature peaks. When x increases from 0.2 to 0.8, the following three features are observed. (1) the α peak does not change. (2) a shoulder peak (denoted as the β peak) appears and grows next to the α peak.

(3) with increasing x, the high-temperature peak (denoted as the γ peak) becomes strong. Thus, we can conclude that Mg$_{1-x}$Cu$_x$Al$_2$O$_4$ contains three types of Cu^{2+} species. Besides, their proportions are related to the value of x (Table 1). Based on the difference in reducibility, we can classify the following three types of Cu^{2+} species: short O-Cu octahedral coordination, elongated O-Cu octahedral coordination, and tetrahedral coordination. The reason for this classification will be discussed.
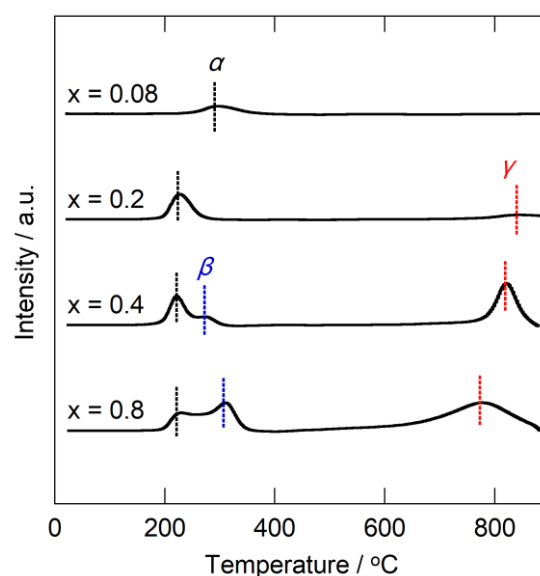

Figure 1 H$_2$-TPR profiles of Mg$_{1-x}$Cu$_x$Al$_2$O$_4$.

Table 1 Peak area in H$_2$-TPR profiles and estimated Cu loading.

x	Peak area in H$_2$-TPR profile [a.u.]				Cu loading [wt%]	
	α	β	γ	Sum	x [a]	H$_2$-TPR [a]
0.08	134	0	0	134	3.5	2.4
0.2	280	0	137	417	8.5	7.3
0.4	265	73	565	903	16	16
0.8	228	389	1110	1727	29	30

[a] The value was used to calculate the Cu loading.

Effects of supports for Pt-based catalysts on conversion of lignocellulosic biomass into aromatic monomers in supercritical water

（AIST*・Tohoku Gakuin University**） ○Kiyoyuki Yamazaki*・
Ryuto Sasaki**・Tatsuya Watanabe**・Satoko Kuwano**・
Naoki Mimura*・Osamu Sato*・Aritomo Yamaguchi*

1. Introduction

Utilization of biomass is effective to realize carbon neutral and sustainable society. Lignin is one of the three components of lignocellulosic biomass as well as cellulose and hemicellulose. Lignin consists of cross-linked aromatic compounds and aromatics can be obtained by depolymerization of lignin.[1]

Lignin conversion to simple aromatic monomers is attractive as an alternative process of conventional reforming from oil resources. In previous works, charcoal supported Pt catalyst was found to be more active than any other charcoal supported metal catalysts for the conversion of biomass to aromatic monomers (Yield=17.4 %).[2] In this study, we considered effects of supports and improved the yield using Pt-based catalysts in supercritical water (Fig.1).
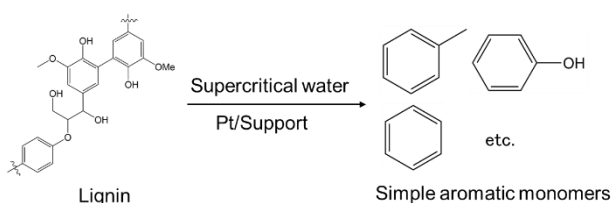

Fig.1 Lignin conversion over supported Pt catalysts

2. Experimental

Supported Pt-based catalysts were prepared as follows. HNO_3 solution of $[Pt(NO_2)_2(NH_3)_2]$, support, and water were put into a flask and stirred overnight. After evaporation of the solvent, obtained powder was reduced with hydrogen in a furnace at 473 K. Then, supported Pt-based catalyst was obtained. The ratio of Pt in Pt-based catalysts was 5wt%.

Lignin conversion was carried out in a batch reactor. Catalyst 0.15 g, Japanese cedar 0.20 g, and water 3.0 g were put into the reactor. Then, the reactor was purged with argon gas and heated at 673 K for 1 h. Gaseous and liquid products were collected and analyzed by gas chromatograph. Solid products were recovered and weighed. Yields of products from lignin conversion were calculated by dividing moles of aromatic compounds in products by moles of aromatic rings in initial biomass.

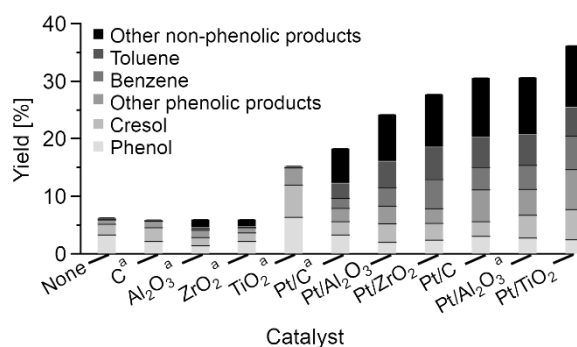## 3. Results and Discussions

Fig.2 Yields of aromatic products from Japanese cedar (a: commercially available)

Fig.2 shows yields of aromatic products in the presence or absence of synthesized or commercial supported Pt catalysts. Various aromatic monomers could be produced by this reaction. Among the catalyst supports (C, Al_2O_3, ZrO_2, and TiO_2), TiO_2 showed catalytic performance even without Pt. Considering the support of the catalyst, TiO_2 was found to be the most effective support in this reaction and the yield was improved up to 36.2 %.

1. J. Zakzeski, et.al., *Chem. Rev.* **2010,** *110*, 3552.
2. A. Yamaguchi, et.al., *Mol. Catal.* **2019,** *477*, 6.

International sess.

[1E04-06] International sess. 2

Chair:Takuya Yoshikawa(Tokyo Metropolitan University)
Thu. Nov 12, 2020 10:45 AM - 11:30 AM Room E (3F/Conf. Room E1-2)

[1E04] Role of acid sites for selective catalytic oxidation of NH_3: the case of niobium oxide supported precious metals catalysts

○Mingyue Lin[1], Baoxiang An[1], Takashi Takei[1], Tetsuya Shishido[1], Tamao Ishida[1], Masatake Haruta[1], Toru Murayama[1,2]　(1. Tokyo Metropolitan University, 2. Yantai University)

10:45 AM - 11:00 AM

[1E05] **Reductive Amination of HMF over Beta Zeolite-supported Ruthenium bimetallic Catalyst**

○Xinyue Li[1], Son Dinh Le[1], Shun Nishimura[1]　(1. Japan Advanced Institute of Science and Technology)

11:00 AM - 11:15 AM

[1E06] Reaction mechanism of dechlorination of chlorofluoroalkene by hydrogen gas over intermetallic compound catalysts

○Tomoaki TAKAYAMA[1], Satoshi ARIYAMA[1], Taku YAMADA[2], Takayuki KOMATSU[1]　(1. Tokyo Institute of Technology, 2. AGC Inc.)

11:15 AM - 11:30 AM

Role of acid sites for selective catalytic oxidation of NH₃: the case of niobium oxide supported precious metals catalysts

(Tokyo Metropolitan University[*1], Yantai University[*2])

○Mingyue Lin[*1], Baoxiang An[*1], Takashi Takei[*1], Tetsuya Shishido[*1], Tamao Ishida[*1], Masatake Haruta[*1], Toru Murayama[*1,2]

1. Introduction

Ammonia is a strong N-containing odor that has negative impacts on human health and the environment. Selective catalytic oxidation (SCO) of NH_3 to N_2 and H_2O is an ideal method for its removal.

NH_3, as an odor gas which has negative impacts on human health and the environment, it is essential and important to develop efficient method to remove it.

Selective catalytic oxidation (SCO) of NH_3 to N_2 and H_2O is an ideal method. However, the developed catalysts either need high reaction temperatures or produce non-environmental-friendly byproduct of N_2O. In this study, we reported the role of acid sites for highly selective catalytic oxidation of NH_3 to N_2 over niobium oxide supported precious metals (Pt, Pd, and Au) catalysts (>95% at the full conversion), which will provide a new concept for the design of catalysts for NH_3-SCO with high N_2 selectivity.

2. Experimental

Nb_2O_5 was synthesized by a hydrothermal synthesis and calcined at 400ºC. [1] Au/Nb_2O_5 was prepared by a sol immobilization method. [1] Pt/Nb_2O_5 and Pd/Nb_2O_5 were prepared by impregnation method. [2] The loading amount of precious metals was prepared as 1wt%. NaOH treatment was carried out by adding 1 mol L^{-1} NaOH (10 mL) to the catalyst and the mixture was stirred for 1 h. After thoroughly washed by deionized water, the resulting solid was dried at 120ºC overnight.

The catalytic activity test was carried out on a fixed-bed reactor system connected with an FI-IR. The inlet gas contained 50 ppm NH_3, 20% O_2, and Ar balance. The total flow rate is 100 mL min^{-1} and the catalyst amount was 0.15 g.

3. Results and Discussion

Niobium oxide obtained from the hydrothermal synthesis shows a deformed orthorhombic structure and its BET surface area was 208 m^2/g. The total acid amount calculated from NH_3-TPD measurements was 0.37 mmol/g and it possessed both Brønsted and Lewis acid sites according to the pyridine adsorption.

The effects of solid acidity of the Nb_2O_5 support on NH_3-SCO were investigated by using NaOH to neutralize the Brønsted acid sites of Nb_2O_5. As shown in Figure 1, Au/Nb_2O_5, Pt/Nb_2O_5, and Pd/Nb_2O_5 showed very high N_2 selectivities along with the increasing NH_3 conversions and they showed 95%, 98%, and 100% N_2 selectivity at the full NH_3 conversion, respectively. After NaOH treatment the N_2 selectivities of Au/Nb_2O_5, Pt/Nb_2O_5, and Pd/Nb_2O_5 decreased significantly which decreased to 32%, 74%, and 74% at the full conversion of NH_3, respectively. These results strongly indicated that the Brønsted acid sites are important for improving the N_2 selectivity of NH_3-SCO.
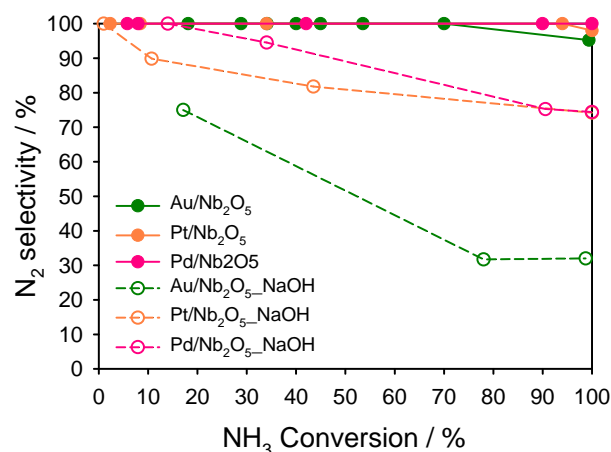

Figure 1. Effect of NaOH treatment on NH_3 conversion and N_2 selectivity over Au/Nb_2O_5, Pt/Nb_2O_5, and Pd/Nb_2O_5.

1) M. Lin, B. An, N. Niimi, Y. Jikihara, T. Nakayama, T. Honma, T. Takei, T. Shishido, T. Ishida, M. Haruta, T. Murayama, *ACS Catal.*, 9(3), 1753 (2019)
2) M. Lin, B. An, T. Takei, T. Shishido, T. Ishida, M. Haruta, T. Murayama, *J. Catal.*, 389, 366-374 (2020).

Reductive amination of HMF over beta zeolite-supported ruthenium bimetallic catalyst

(JAIST) ○LI, Xinyue・LE, Dinh Son・NISHIMURA, Shun

1. Introduction

The ever-increasing industrial production of commodity and specialty chemicals inexorably depletes the finite primary fossil resources available on Earth. Consequently, for the sustainable development, effective transformations of renewable biomass, which is a virtually inexhaustible reservoir, to fuels and chemical building blocks are envisaged.[1] The 5-hydroxymethyl-2-furaldehyde (HMF) is a great platform chemical produced from lignocellulosic biomass, and enables various successive transformations to value-added compounds. Herein, the reductive amination of HMF over various beta zeolite supported monometallic and bimetallic Ru catalysts, denoted as Ru/BEA and RuM/BEA, to 5-aminomethyl-2-furylmethanol (FAA) is investigated. Primary amines are important and versatile building blocks in organic synthesis because they are widely utilized as intermediates for the production of polymers, drugs, dyes, and detergents.[2-4]

2. Experimental

The catalysts were prepared by an impregnation method with various BEA composed with different Si/2Al ratios (42.4, 104, 150, 440, and 1700). To evaluate the catalytic performance, HMF (1 mmol), 25% NH_3 aq. (3 mL), and ethanol (3 mL) were mixed in a stainless-steel autoclave with a Teflon inter tube (50 mL vol.). After addition of as-prepared catalyst (10 mg) and filling with H_2 gas (0.6 MPa), the reaction was performed at 100 °C under vigorous stirring. The reaction media is analyzed by a GC-FID equipped with a nonpolar DB-1 column by using 1-butanol (1 mmol) as an internal standard.

3. Results and Discussions

At first, various Ru metal loadings on BEA zeolite are surveyed at Si/2Al = 150. It is observed that increase of Ru loading leads an increase of FAA yield gradually, and then both 3wt% and 5wt% of Ru loaded BEA catalysts gave the high FAA yields of 70%.

Figure 1 (a) shows the time-based reaction progress over 3wt% monometallic Ru/BEA composed with different Si/2Al ratios. Interestingly, the Si/2Al ratio of BEA support significantly impacted the reactivity for the reductive amination of HMF. Increase of Si/2Al from 42.2 to 150 has enhanced the reactivity for FAA production, and the highest yield for FAA was obtained as 70% for 6 h reaction. While, further increase of Si/2Al lead a drastic decrease of FAA yield. Analyses of Ru-K edge XAFS (SPring-8, BL01B1 and BL14B2) indicated that smaller Ru-Ru CNs served higher yield

of FAA. It is also observed that highly active Ru/BEA (Si/Al2 = 150) possesses more fraction of Ru-O than that of low active Ru/BEA (Si/2Al = 1700). According to these results, it is expected that the Si/2Al ratio of BEA support contributed to the metal-support interaction, and which played a key factor to control Ru size leading to difference in reactivity for the reductive amination of HMF to FAA.

To further enhance the reactivity of monometallic Ru/BEA catalyst and decrease the quantity of precious Ru element usage, addition of common elements such as Fe, Cu, Co and Ni constructing bimetallic RuM/BEA (Si/2Al = 150) was investigated. Remarkably, the bimetallic RuNi was found to be the superior catalyst among those combinations; which served 70% yield of FAA whereas RuFe, RuCo and RuCu presented only 17-47% yield of FAA at 12 h reaction (**Figure 1(b)**).
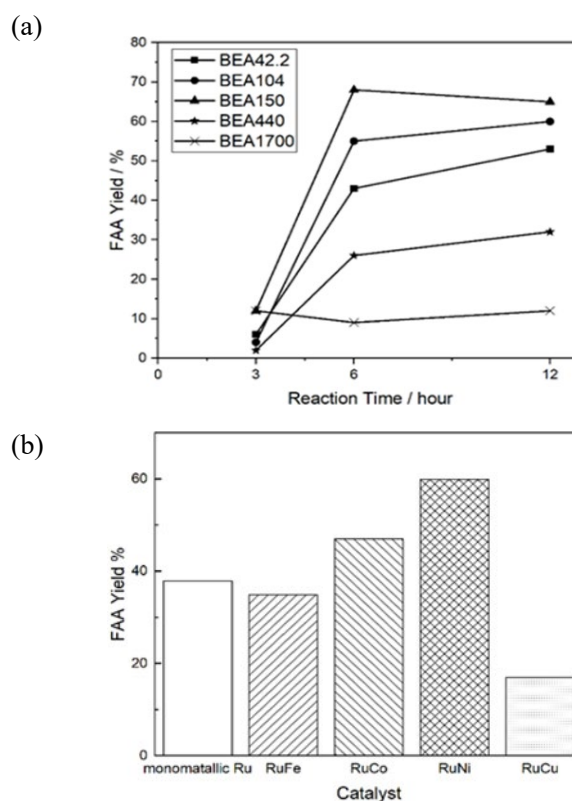
(a)

(b)

Fig. 1 Yield of FAA on the reductive amination of HMF for (a) Time-based reaction progression over the 3wt% Ru/BEA composed of different Si/2Al ratio, and (b) 12 h reaction over various RuM/BEA catalysts.

1) Gérardy *et al.*, *Chem. Rev.* 120 (2020) 7219.
2) Nisimura *et al.*, *Res. Chem. Intermed.* 42 (2016) 19.
3) Komanoya *et al.*, *J. Am. Chem. Soc.* 139 (2017) 11493.
4) Dong *et al.*, *Mol Catal.* 482 (2020) 110755.

Reaction mechanism of dechlorination of chlorofluoroalkene by hydrogen gas over intermetallic compound catalysts

(Tokyo Institute of Technology 1*, AGC Inc. 2**)　○Tomoaki TAKAYAMA 1*,

Satoshi ARIYAMA 1*, Taku YAMADA 2**, Takayuki KOMATSU 1*

1. Introduction

2,3,3,3-tetrafluoropropene (**H(2)**, scheme 1) has gathered much attention as an alternative automobile refrigerant to the current ones because of its lower global warming potential.[1] Dechlorination of chlorofluoroalkene, **H(0)**, by hydrogen gas over heterogeneous Pd catalyst has been known as a protocol to provide **H(2)**. However, by-products, **H(3)~H(5)**, have been formed *via* the successive hydrogenation and defluorination of **H(2)**. In contrast, we have recently discovered that Pd-based intermetallic compounds (Pd$_3$M; M = Bi, Pb, or In) inhibit the by-products from producing.[2] Herein, we discuss the factor affecting the selectivities to the products in the dechlorination of **H(0)** based on control and spectroscopic experiments.
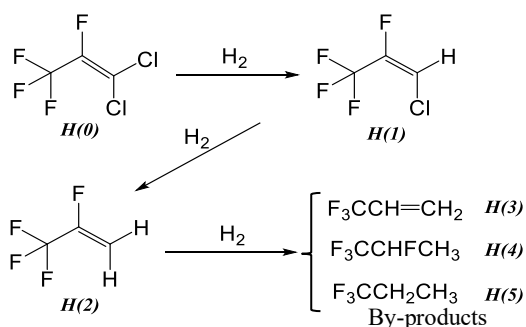
Scheme 1. Dechlorination of **H(0)** by hydrogen gas.

2. Experimental

The nanoparticulate monometallic Pd and intermetallic compounds Pd$_3$M (M = Bi, Pb, or In) were formed on SiO$_2$ support by co-impregnation with the conventional pore-filling protocol, followed by H$_2$ reduction at 400 and 800ºC. Dechlorination of **H(0)** was carried out by a fixed-bed flow-type stainless steel reactor (atmospheric pressure). Prior to the dechlorination reaction, the catalysts fixed on the bed were reduced by H$_2$ gas at 400ºC, followed by cooling to room temperature. The reaction was initiated by supplying mixed gas (**H(0)**/H$_2$/Ar=1/1/3.4; mole ratio) at 90 or 150ºC. The products were determined by injecting the gaseous sample extracted using a glass syringe into GC-FID.

3. Results and Discussion

Fig 1. shows influence of the conversion of **H(0)** on the selectivities to **H(1)** and **H(2)** formations. The selectivities over all the Pd-based intermetallic compound catalysts were greater than that over monometallic Pd catalyst. Among them, Pd$_3$Bi showed the highest selectivity. In other words, the formations of the by-products, **H(3)~H(5)**, were inhibited over Pd$_3$Bi as compared to those on the other intermetallic compound catalysts.

We investigated the relationship between electron density of the Pd sites of the Pd-based catalyst surfaces and the by-product selectivities based on Fourier transform infrared spectroscopy using CO as the probe molecule. The sum of the selectivities to **H(4)** and **H(5)** formations were certainly decreased with red-shift of the wavenumber of the stretching vibration of CO, which could be assigned to linear adsorption of the CO molecules on the Pd sites (Fig. 2), while no relationship was observed against the sum of the **H(3)** and **H(5)** selectivities (data not shown). This suggests that the electron density of the Pd sites makes a difference in inhibition of the successive hydrogenation of the alkenyl group.
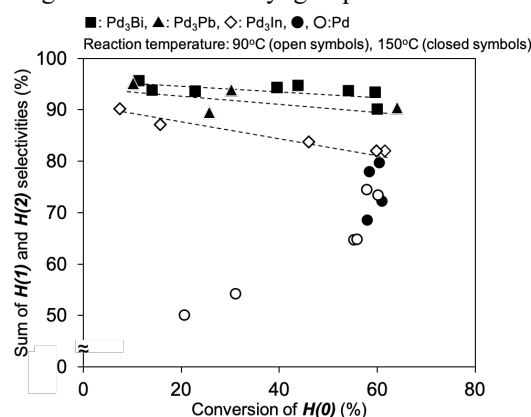

Fig. 1 Influence of the conversion of **H(0)** on the sum of **H(1)** and **H(2)** selectivities.
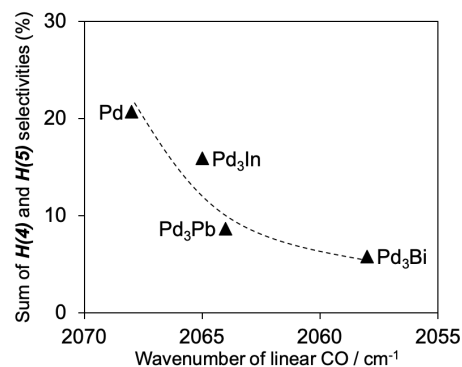

Fig. 2 Relationship between wavenumber of CO adsorbed on the Pd sites and the sum of **H(4)** and **H(5)** selectivities.

1) Calm, J. M., *Int. J. Refrig.* **31**, 1123 (2008).
2) Ariyama, S., Takayama, T., Yamada, T., Komatsu, T., 124th CATSJ Meetings Abstract, 2E11 (2019).

International sess.

[1E07-09] International sess. 3

Chair:Tomoaki TAKAYAMA(Tokyo Institute of Technology)
Thu. Nov 12, 2020 1:00 PM - 2:00 PM Room E (3F/Conf. Room E1-2)

[1E07] Development of Ni-Ir alloy catalyst for hydrogenation of unsaturated compounds

○Masazumi Tamura[1] (1. Osaka City University)
 1:00 PM - 1:30 PM

[1E08] Hydroxyapatite supported polyvinylpyrrolidone-capped CuPd bimetallic catalyst for highly selective γ-butyrolactone *via* hydrogenation of succinic acid

○Son Dinh Le[1], Shun Nishimura[1] (1. Graduate School of Advanced Science and Technology, Japan Advanced Institute of Science and Technology)
 1:30 PM - 1:45 PM

[1E09] Ultrastable and selective catalyst for propane dehydrogenation using Pb-modified PtGa alloy

Yuki Nakaya[1], Ken-ichi Shimizu[1], ○Shinya Furukawa[1] (1. Institute for Catalysis, Hokkaido University)
 1:45 PM - 2:00 PM

Development of Ni-Ir alloy catalyst for hydrogenation of unsaturated compounds

（Osaka City University） ○Masazumi Tamura

1. Introduction

Catalytic hydrogenation of unsaturated compounds with gaseous H_2 is widely used in petrochemical, coal chemical and fine chemical industries, and development of effective heterogeneous catalysts is highly required because of the durability, recyclability, easy separation of catalysts from the products. To achieve economic and low-energy processes, rational design and preparation of heterogeneous catalysts with high atomic efficiency are essential, and various approaches such as control of geometric and electronic structure, formation of alloys, intermetallic compounds or core-shell structures, modification of main metals with metal oxides, metal ions or organic compounds, and so on. Among these approaches, the formation of bimetallic alloys is a powerful tool for fine tuning of the activity and selectivity, and particularly, single-atom alloys (SAAs) are promising owing to the high atomic efficiency[1]. SAAs often show unique and/or superior catalytic performance in comparison with the monometallic counterparts due to the comparatively well-defined active sites as well as assisting effect of the mother metals. SAAs with noble metals such as Pd, Pt, Au single-atom alloys have been intensively developed, however, SAAs with base metals such as Ni, Cu, Co and Fe single-atom alloys are hardly reported. However, the base metals often show unique catalytic performance in organic reactions, and particularly it is well-known that Ni metal works as a good catalyst for hydrogenation reactions. In this study, we aimed at the development of effective Ni-based catalysts for hydrogenation reactions. We found that Ni single-atom in Ni-Ir alloy showed high catalytic activity and high selectivity to hydrogenation reactions of unsaturated compounds compared with the monometallic counterpart catalysts[2].

2. Experimental

Ir-Ni/SiO2 (Ir: 4 wt%) was prepared as follows: Ir/SiO2 was prepared by impregnating SiO2 with H_2IrCl_6 aqueous solution, followed by drying in oven at 373 K overnight.

Ni was loaded on the dried Ir/SiO2 with aqueous $Ni(NO_3)_2$ solution in the same method as the case of Ir/SiO2, and the obtained dried catalyst was calcined at 773 K for 3 h. The catalyst was reduced under H_2 flow (30 ml/min) at 773 K for 1 h before activity test. Appropriate amount of the reduced catalyst, styrene and methanol solvent were added into a 190 ml autoclave with an inner glass cylinder. The air was purged by flushing three times with H_2, and then the reaction was performed at 303 K and 8 MPa H_2. The products were analyzed by FID-GC and GC-MS.

3. Results and discussion

The performance of SiO2-supported nickel and iridium catalysts with different Ni/Ir molar ratios (Ni–Ir/SiO2-X, X=Ni/Ir molar ratio) was investigated in hydrogenation of styrene as a model reaction. Ni-Ir/SiO2 with Ni/Ir molar ratio of 1 (Ni-Ir/SiO2-1) showed the highest conversion among the Ni-Ir/SiO2-X catalysts, and the ethylbenzene was obtained in high selectivity (>99%). The reaction rate per total catalyst weight (160 mmol min^{-1} g^{-1}) is more than 7-fold higher than those of the monometallic counterpart catalysts (Figure 1). The reusability of the Ni-Ir/SiO2-1 was confirmed by four-time reuse tests, and
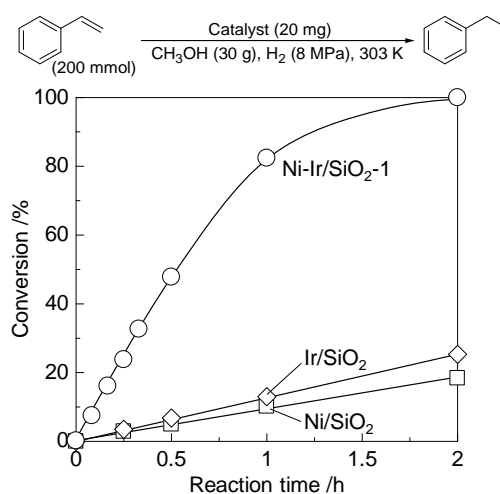

Figure 1 Time-courses of hydrogenation of styrene with Ni-Ir/SiO2-1, Ir/SiO2 (Ir: 4 wt%) and Ni/SiO2 (Ni: 1.2 wt%) catalysts. Reaction conditions: catalyst 20 mg, styrene 200 mmol, CH3OH 30 g, H_2 8 MPa, 303 K.

it was also confirmed that the catalyst structure was not changed during reaction by XRD and XAS analyses.

The characterization of Ni–Ir/SiO$_2$-1 by XRD, TPR, XAFS and TEM showed that the catalyst was composed of Ni–Ir alloys and Ni particles, and the average particle size of the Ni–Ir alloy was estimated to be ~3 nm (Figure 2). The alloy composition (Ni/(Ni+Ir)) of Ni-Ir alloy in Ni-Ir/SiO$_2$-1 catalyst was calculated based on Vegard's law to be 0.24 from the Ni-Ir alloy peak position of XRD patterns of Ni–Ir/SiO$_2$-1 catalyst, which was also supported by EDX line analysis of the TEM image (Figure 2).
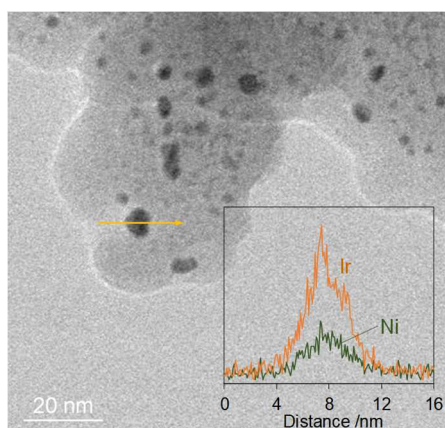

Figure 2 TEM image and EDX line analysis of Ni-Ir/SiO$_2$-1 catalyst after reduction.

The relationship between the turnover frequency based on the number of surface metal atoms (TOFs (min^{-1})) and alloy composition of Ni/(Ni+Ir) of Ni-Ir/SiO$_2$-X catalysts was investigated, and the result is shown in Figure 3. The TOFs increased with increasing the alloy composition up to 0.16, reaching a maximum TOFs of 4190 min^{-1}. However, the TOFs decreased at higher alloy compositions, suggesting that the high Ni content in the Ni-Ir alloys is not preferable for the reaction. The isolated Ni amount in Ni-Ir alloys with various Ni loading amount was estimated by the random model, which is called, ideal isolated Ni atom amount, and it is plotted as a function of the alloy composition of Ni/(Ni+Ir) (Figure 3). The change of the ideal isolated Ni amount is quite similar to that of the TOFs (Figure 3). These results strongly suggest that the isolated Ni atom in the Ni–Ir alloy can be the main active site for the reaction.

Finally, the applicability of the Ni-Ir alloy catalyst to hydrogenation of various unsaturated compounds was studied. Ni-Ir/SiO$_2$-1 showed higher activity to
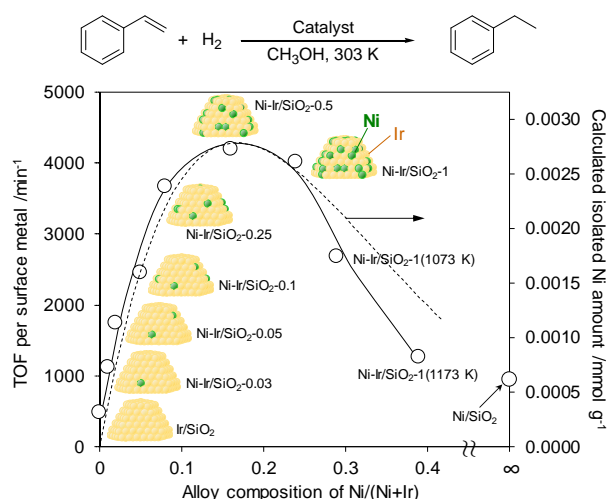

Figure 3 Relationship between alloy composition of Ni/(Ni+Ir) in Ni-Ir/SiO$_2$-X catalysts and TOF per surface metal (TOFs, solid line), ideal isolated Ni atom amount (dotted line) and images of alloys.

hydrogenation of various styrene derivatives with electron-donating and electron-withdrawing functional groups, 1-octene, a terminal olefin and 2-octene, an inner olefin, than the monometallic counterpart catalysts. On the other hand, the activity enhancement was not observed in hydrogenation of ethylbenezene, namely the catalyst is not suitable for hydrogenation of the aromatic ring. However, Ni-Ir/SiO$_2$-1 catalyst showed higher activity to hydrogenation of pyridine than the monometallic counterpart catalysts. The reaction mechanisms of hydrogenation of olefins, the benzene ring and pyridine ring over Ni-Ir/SiO$_2$ catalyst may be different. The details of the reaction mechanism will be discussed in the presentation.

We found that SiO$_2$-supported Ni-Ir alloy showed much higher activity for hydrogenation of olefins than the monometallic counterpart catalysts such as Ni/SiO$_2$ and Ir/SiO$_2$, and based on the catalyst characterization and kinetic studies, Ni single-atom in Ni-Ir alloy is responsible for the high activity.

1) P. Liu, Y. Zhao, R. Qin, S. Mo, G. Chen, L. Gu, D. M. Chevrier, P. Zhang, Q. Guo, D. Zang, B. Wu, G. Fu, N. Zheng, *Science*, 352 (2016) 797-801.
2) J. Bai, M. Tamura, Y. Nakagawa, K. Tomishige, *Chem. Commun.*, 55 (2019) 10519 - 10522.

Hydroxyapatite Supported Polyvinylpyrrolidone-Capped CuPd Bimetallic Catalysts for Highly Selective γ-Butyrolactone *via* Hydrogenation of Succinic Acid

（JAIST）○LE, Dinh Son・NISHIMURA, Shun

1. Introduction

Succinic acid (SA) was identified as one of the most potential platform chemicals which can be converted to a number of value-added products.[1] The main types of SA conversions include hydrogenation, reductive amination, and esterification.[2] The catalytic hydrogenation toward γ-butyrolactone (GBL), 1,4-butanediol (BDO), and tetrahydrofuran (THF) is the most attractive conversion route; the manufacture of these expected to account for nearly one-third of the SA production in 2020.[3] In the present work, poly(N-vinylpyrrolidone) (PVP)-capped CuPd NPs stabilized on hydroxyapatite (HAP) is studied for the hydrogenation of SA to afford highly selective GBL.

2. Experimental

The Cu_xPd_y–PVP/HAP (x+y = 0.1 mmol) catalysts were prepared using polyol reduction method with 2-ethoxyethanol as a reducing agent. The catalysts were examined by extensive characterizations including X-ray diffraction (XRD), transmission electron microscopy (TEM), X-ray photoelectron spectra (XPS), and X-ray absorption fine structure (XAFS, Saga-LS, No. 1910092R).

Typically, a solution including 1,4-dioxane (10 mL), SA (0.1 g), and the catalyst (0.1 g) was loaded into an autoclave. The reactor was purged with pure H_2 before being pressurized to the target pressure at room temperature. Thereafter, the reactor was heated at 200 °C for 48 h under vigorous stirring. After reaction, the reaction media was centrifuged and analyzed by gas chromatography with a DB-FFAP column and a high-performance liquid chromatography using an Aminex HPX-87H column.
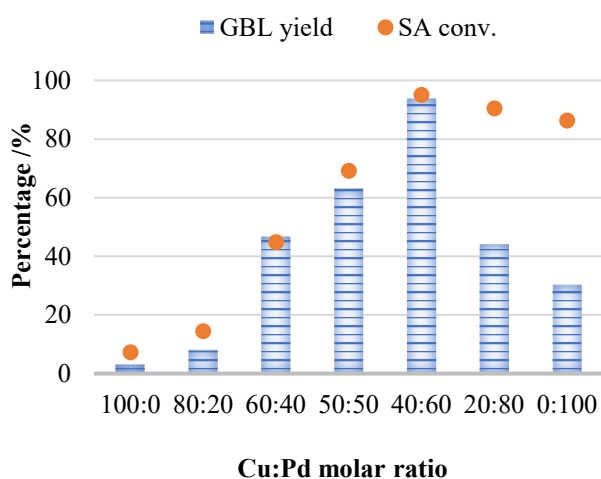

Figure 1. Effects of Cu:Pd ratio on the hydrogenation of SA over the Cu_xPd_y–PVP/HAP

3. Results and Discussions

Figure 1 shows the trend of hydrogenation of SA over the Cu_xPd_y-PVP/HAP with different Cu:Pd ratios. The monometallic Cu exhibited low activity, while the addition of Pd resulted in better catalytic performance; the SA conversion and GBL yield increased and reached its peak over the $Cu_{40}Pd_{60}$. Interestingly, further addition of Pd in this bimetallic system caused a significant drop in the GBL selectivity. The Pd monometallic catalyst exhibited lower activity and GBL selectivity. These results suggest that the close interaction between Cu and Pd, i.e., alloying, is responsible for the enhancement of catalytic activity and selectivity on the Cu_xPd_y–PVP/HAP catalyst.

The Pd-K edge XAFS results are shown in **Figure 2**. The monometallic Pd_{100} catalyst represents the Pd–Pd metallic peak of Pd foil at 2.74 Å. Upon addition of Cu, another peak was observed at lower position (2.54 Å), indicating the formation of Cu–Pd bonds of CuPd alloy.[4] Except for the Pd_{80} catalyst with low Cu concentration, the coordination numbers (CNs) of Pd–Cu increased with the increase of Cu concentration, indicating the increase in alloying degree. However, the Pd-Cu CNs did not explain the trend of catalytic performance for SA hydrogenation as shown in **Figure 1**. It is considered that the presence of isolated Pd in Pd rich CuPd alloy would account for the superior activity on the SA hydrogenation to highly selective GBL.
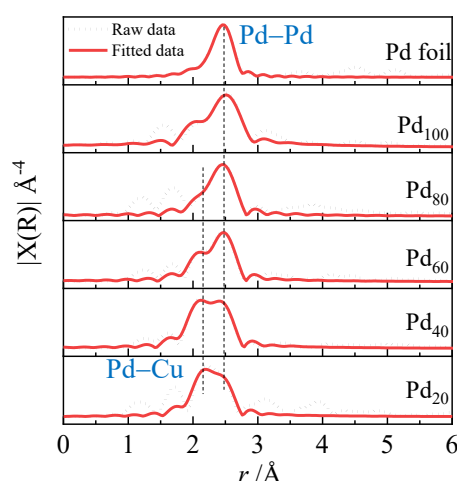

Figure 2. FT EXAFS fitting results at Pd K-edge.

1) A. Corma *et al.*, *Chem. Rev.*, **107**, 2411 (2007)
2) A. Mazière *et al.*, *Biofuels, Bioprod. Biorefining*, **11**, 908 (2017)
3) C. Delhomme *et al.*, *Green Chem.*, **11**, 13 (2009)
4) F. Xing et al., *Chem. Sci.*, **10**, 8292 (2019)

Ultrastable and selective catalyst for propane dehydrogenation using Pb-modified PtGa alloy

(Hokkaido Univ.) Yuki Nakaya, Ken-ichi Shimizu, Shinya Furukawa

1. Introduction

Propylene is an important raw material for plastics, synthetic rubber, surfactants, dyes and pharmaceuticals. In recent years, there has been increased demand for propylene produced from cheaper, shale-originated propane. Reaction temperatures of more than 600°C are necessary to obtain sufficient propylene yields, but under these harsh conditions, severe catalyst deactivation is inevitable due to carbon deposition and/or sintering. Catalysts in practical use, therefore, must be regenerated continuously or in short cycles, making the process inefficient and costly.

In this study, we developed an ultrastable and selective catalyst for propane dehydrogenation using a Pb-modified PtGa alloy that worked for 96 h without deactivation even at 600°C.[1]

2. Experiment

Catalysts were prepared by co-impregnation method using silica (CARiACT G-6, Fuji Silysia) as a catalyst support (Pt loading: 3 wt%, Pt : Ga : Pb = 1 : 1 : 0.5). Propane dehydrogenation was carried out in a fix-bed continuous-flow reaction using quartz tube under atmospheric pressure at 600C (C_3H_8 : H_2 : He = 3.9 : 5 : 40 mL/min, catalyst: 15 mg, quartz sand 1.5 g).

3. Results and Discussion

Fig. 1 shows the catalytic performance of Pt-based catalysts. $PtGa/SiO_2$ and Pt_3Sn/SiO_2, which are known as selective catalysts for propane dehydrogenation, showed rapid deactivation within 10 h. In contrast, PtGa–Pb/SiO_2 retained the high propane conversion (30%) and propylene selectivity (99.6%) for 96 h (Fig. 2). The deactivation rate constant (kd) was 0.001 h^{-1}, which is the lowest value ever reported for propane dehydrogenation performed at >580°C. Thus, we successfully developed an ultrastable and selective catalyst for propane dehydrogenation.

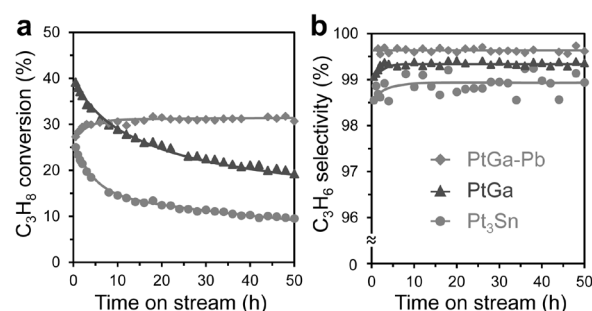FT-IR study with CO adsorption and DFT simulation for adsorbed CO revealed that (1)

Fig. 1 Changes in propane conversion (**a**) and propylene selectivity (**b**) in propane dehydrogenation. Catalyst amount was adjusted so that the number of exposed Pt was identical (4.5 µmol): PtGa (9.0 mg), PtGa–Pb) (15 mg), Pt_3Sn (3.7 mg), and diluted with quartz sand (total 1.5 g). Gas feed: C_3H_8:H_2:He = 3.9:5.0:40 mL min^{-1}. Temperature: 600°C.
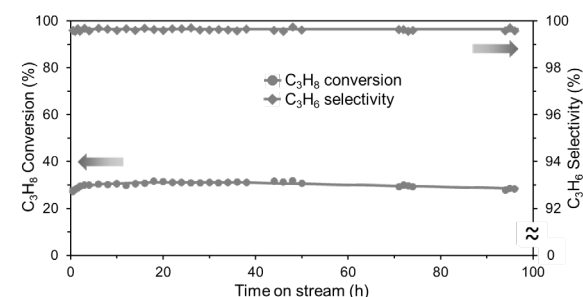

Fig. 2. Long-term stability test for PtGa–Pb/SiO_2.

PtGa alloys had single-atom-like isolated Pt_1 site surrounded by inert Ga and three-fold Pt_3 ensemble sites, and (2) the Pt_3 sites were selectively blocked by Pb deposition, while the Pt_1 sites remained intact. Comprehensive DFT calculation also indicated that the Pt_3 site was active not only for propane conversion to propylene but also for propylene decomposition, whereas Pt_1 site selectively catalyed propane conversion to propylene (propylene decomposition was effectively inhibited).

We also confirmed that the Pb-modified PtGa alloy nanoparticles were not sintered after the long-term use and the spent catalyst could be regenerated by O_2 treatment (calcination) and the subsequent H_2 reduction.

1. Y. Nakaya, J. Hirayama, S. Yamazoe, K. Shimizu, S. Furukawa, *Nat. Commun.*, **2020**, *11*, 2838.

International sess.

[1E10-11] International sess. 4

Chair:Shun Nishimura(Japan Advanced Institute of Science and Technology)

Thu. Nov 12, 2020 2:15 PM - 3:00 PM Room E (3F/Conf. Room E1-2)

[1E10] Synthesis of zeolitic Mo-doped vanadotungstate materials with tailorable oxidability and acidity

○Meilin Tao[1], Satoshi Ishikawa[1], Wataru Ueda[1]　(1. Faculty of engineering, department of material and life chemistry, Kanagawa University)

　2:15 PM - 2:30 PM

[1E11] Development of nano-structured catalyst using oxide nanosheets

○Shintaro Ida[1]　(1. Institute of Industrial Nanomaterials, Kumamoto University)

　2:30 PM - 3:00 PM

Synthesis of zeolitic Mo-doped vanadotungstate materials with tailorable oxidability and acidity

(Kanagawa Univ.) ○ TAO, Meilin ・ ISHIKAWA, Satoshi ・ UEDA, Wataru∗

1. Introduction

Ordered porous transition metal oxides are more and more attractive because of their structure-based properties such as porosity and redox property. Previously, our group reported a kind of microporous zeolitic transition metal oxides ($W_{4.0}V_{3.0}O_{19}$; **VT-1**), which is composed of cubane clusters $[W_4O_{16}]^{8-}$ and VO^{2+} linkers (**Fig. 1**) [1]. Here we successfully prepared a series of transition metal substituted VT-1 materials, in which some of W in cubane unit was replaced by Mo, and V was substituted with Ti and Zr.
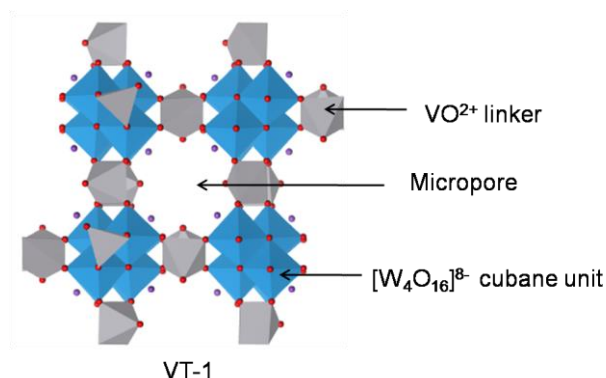

Fig. 1. Structural model of VT-1

2. Experimental

Mo_xW_{4-x} was obtained by hydrothermal synthesis (175 °C, 24 h) of the mixture of $(NH_4)_6H_2W_{12}O_{40}$, $(NH_4)_6Mo_7O_{24}$, and hydrated $VOSO_4$ under the pH of 4.0. $Mo_{0.7}W_{3.3}(Ti$ or $Zr)_yV_{(3.0-y)}O_{19}$ were prepared by dispersing $Mo_{0.7}W_{3.3}$ in the aqueous solution of $Ti(SO_4)_2$ and $Zr(SO_4)_2$ with desired concentration.

3. Results and Discussion

From the ICP results, the addition of Mo caused the decrease of W in the unit cell, while the amount of V remained unchanged (**Fig. 2**). Based on DFT calculation, the stability of the Mo containing VT-1 materials decreased as the increase of Mo amount. The maximum doping amount of Mo was 1.0 ($W_{3.0}Mo_{1.0}V_{3.0}O_{19}$), and increasing Mo resulted in the formation of an unknown phase.

Then, we treated VT-1 and $Mo_{0.7}W_{3.3}$ with H_2SO_4 solution and the elemental compositions after the treatment were investigated by ICP (**Fig. 3a**). We found that the amount of V decreased with the decrease of pH
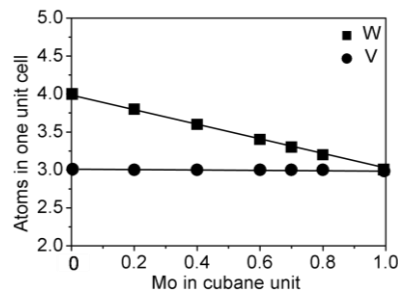

Fig. 2. The changes of W and V amount as a function of x in Mo_xW_{4-x} unit

in the solution and the rate of decrease of V was much faster in $Mo_{0.7}W_{3.3}$ than that of VT-1. We speculated that V in Mo_xW_{4-x} was leached out by hydration easier than that of VT-1 when decreasing the pH of the solution. The leaching of V from the structure caused the loss of the crystallinity as confirmed by XRD measurements. However, the crystallinity was remained unchanged when Ti or Zr source was added in the acid solution despite the leaching of V from the VT-1 structure. Interestingly, Ti or Zr was introduced into the VT-1 structure with the compensated amount of V leached out and the sum of V and Ti or Zr in the VT-1 structure was always 3.0, indicating that Ti or Zr is introduced into the V site leached out by the acid treatment (**Fig. 3b**). Maximum amount of Ti or Zr introducible into the structure was 1.0 in the VT-1 unit cell.
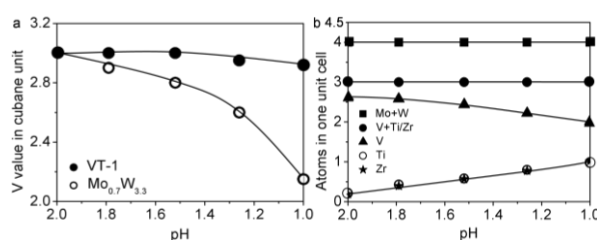

Fig. 3. Changes of the number of atoms in the VT-1 structure as a function of pH of the solution: a) in H_2SO_4 solution; b) in $Ti(SO_4)_2$ or $Zr(SO_4)_2$ solution.

FT-IR, Raman, and UV-Vis spectra further confirmed the successful introduction of Mo, Ti and Zr into the VT-1 structure. In the presentation, the physicochemical properties and catalytic activities over $Mo_xW_{(4-x)}(Ti$ or $Zr)_yV_{(3.0-y)}O_{19}$ for NH_3-SCR will be discussed.

1) Z. Zhang, et al, *Nat. Commun*. **9**, 3789 (2018).

Development of nano-structured catalyst using oxide nanosheets

Kumamto Univerisity ○Shintaro Ida

Introduction

Some of layered compounds can be exfoliated into two-dimensional materials, so called nanosheets, with a thickness of around 1nm. Such nanosheets are used as building blocks to prepare well-ordered nano-structure such as super-lattice structure and pn-junction. In our study, we have been focusing on the activities of photocatalyst, and electrode catalyst of nano-structured catalysts prepared using nanosheets Hydrogen production from water using a photocatalyst and solar energy is the ultimate goal in renewable energy research [1]. Various oxides and oxynitrides have been reported as potential photocatalysts capable of decomposing water. However, there are several issues preventing their practical application, such as low quantum efficiency in the visible light region. One factor that causes a decrease in the photocatalytic activity is a recombination reaction between the electron and hole. When a photocatalyst is illuminated by light with an energy greater than the bandgap energy, a photo-excited electron and hole are generated within the powder. In order for these carriers generated within the powder to react with water, they must travel a long distance to the surface. During this trip, they may recombine or get trapped at defect sites. One ideal material that can suppress the recombination and provide a short travel distance is a semiconducting nanocrystal without inner and surface defects. However, in order to accomplish four-electron oxidation of water into oxygen on a 1 nm-diameter nanocrystal, one nanocrystal particle must absorb four photons with sufficient energy in a remarkably short time. Thus, it may be impossible to obtain sufficient photon flux density to meet requirements for solar energy.

A two-dimensional structure may satisfy the requirement described above. Specifically, a two-dimensional crystal (nanosheet) prepared by exfoliation of a layered compound is a single crystal with a homogeneous ultrathin thickness, and has a lateral dimension of several hundred nanometers to several micrometers. Therefore, the travel distance of the photo-excited carriers is short, and many photons can be absorbed by the nanosheet in a remarkably short time under low photon flux density due to its large section area. Recently, there have been many reports on p-type and n-type semiconducting nanosheets and nanosheet photocatalysts with visible light response, and studies on nanosheet photocatalysts have been becoming more frequent. The characteristic performance of nanosheet photocatalysts has been reported. For instance, it is well known that a photocatalyst without co-catalyst loading

has poor photocatalytic activity for water splitting. However, a particular type of oxide nanosheet shows a high photocatalytic activity for hydrogen evolution from water without co-catalyst loading. A graphene-based photocatalyst is also a candidate photocatalyst, and new insights on photocatalytic reactions have been reported. Thus, the two-dimensional structure is expected to contribute to the development of photocatalysts for water splitting in the future. In this talk, e provides a short overview of recent research activities related to oxide nanosheets, nanosheet p-n junction photocatalysts [2], and attractive approaches for understanding the reaction mechanism [3], and electrode catalyst of nano-structured catalysts prepared using nanosheets.

Nanosheet p-n junction surface

The creation of a p-n junction is a strategy to improve photocatalytic activity, since the potential gradient generated by formation of a p-n junction can potentially act to suppress the recombination reaction. The potential gradient on the surface is generated by the diffusion of charge carriers between n-type and p-type semiconducting materials, which is expected to function as a driving force for the photo-excited holes and electrons to move to their respective reduction and oxidation sites. However, advancements in this field have been limited due to the difficulty in the preparation and evaluation of such junction structures. Nanosheets are a potential material to provide an answer to the issue mentioned above. A p-n junction structure without an amorphous layer between different p-type and n-type semiconducting materials with different crystal phases can be prepared by lamination of p-type and n-type semiconducting nanosheets. In the case of nanoparticles, the connection between them is point-to-point, whereas in a nanosheet, the connection is face-to-face. This is one of the advantages of nanosheets in the preparation of p-n junctions.

References:

[1] Takata, T., Jiang, J., Sakata, Y. *et al. Nature,* 581**,** 411–414 (2020).

[2] Awaya, K. Takashiba A., Taniguchi, T. *et al., Chem. Commun.*, 55, 4586-4588 (2019,)

[3] Ida, S. Sato, K., Nagata, T., *et al., Angew. Chem. Int. Ed.,* 57, 9073-9077 (2018)